3792

INSTITUTE OF PHYSICS PUBLISHING
Meas. Sci. Technol. 12 (2001) 345–352

MEASUREMENT SCIENCE AND TECHNOLOGY
www.iop.org/Journals/mt PII: S0957-0233(01)16565-3

Inspection of wood density by spectrophotometry and a diffractive optical element based sensor

Jari Palviainen and Raimo Silvennoinen

Väisälä Laboratory, Department of Physics, University of Joensuu, FIN-80101 Joensuu, Finland

Received 23 August 2000, in final form and accepted for publication 3 January 2001

Abstract

Correlation among gravimetric, spectrophotometric and radiographic data from dried wood samples of Scots pine (*Pinus sylvestris L*) was observed. A diffractive optical element (DOE) based sensor was applied to investigate density variations as well as optical anisotropy inside year rings of the wood samples. The correlation between bulk density of wood and spectrophotometric data (reflectance and transmittance) was investigated for the wavelength range 200–850 nm and the highest correlation was found at wavelengths from 800 to 850 nm. The correlation at this wavelength was smaller than the correlation between bulk density and radiography data. The DOE sensor was found to be capable of sensing anisotropy of the wood samples inside the year ring.

Keywords: wood density, spectrophotometry, diffractive optical element

1. Introduction

The density of wood is directly related to other properties of wood such as hygroscopicity, shrinkage and swelling, mechanical, thermal, acoustical and electrical characteristics [1]. Thus it is important as an index of wood quality. Many parameters affect density properties of wood. Here we refer only to fertilization [2], solar radiation and air temperature [3] and environmental factors [4]. Structural variations in wood density are caused by changes in the proportion of cell wall to cell cavity, which varies during a growing season. The cell walls of latewood regions are observed to be thicker and the cell cavities smaller in comparison with those of earlywood regions [1]. Consequently, the increase in percentage of latewood will increase the bulk density of wood. The proportion of extractives such as gums, fats, resins, sugars, oils, tannins and alkaloids deposited within cell walls and in cavities, varies from less than 1% to 20% or more in oven-dry wood. Also the chemical components of cell walls (e.g. cellulose, hemicellulose and lignin) differ in density. The amount of extractives and the cell wall substance itself have different concentrations in earlywood and latewood regions. Thus, it is important to investigate the intra-ring properties, such as wood density.

This calls for more advanced methods than gravimetric ones, e.g. densitometric methods or x-ray techniques [2, 5, 6]. These methodologies have been developed rapidly in recent years, for various industrial and research purposes, but their industrial applications are still very expensive systems and are not commonly calibrated for the determination of wood properties. Furthermore, very carefully prepared pieces of wood and computerized methods of data storage are needed for these applications. Also wood densities, for example, need to be inferred by correlation of the intensity of x-rays transmitted through the wood to gravimetric density measurements on small samples [6]. Sophisticated tools will be needed in future for intra-ring analysis of wood properties, tools which could give accurate information on such properties as wood density but still be reasonably simple to use and not too costly.

In this work we investigated light components scattered from the wood samples of Scots pine (*Pinus sylvestris L*) for which results of gravimetric density measurements and x-ray negative films were also available. We measured the spectral reflectance and transmittance of the wood samples by using a spectrophotometer (with an integrating sphere) and calculated the correlation coefficients relating the bulk density and optical data as a function of wavelength. Also, a diffractive optical element (DOE), which had already been observed to be effective elsewhere [7], was applied to sense the light components reflected and transmitted from the samples in order to analyse anisotropy [8] and variation of density [9].

0957-0233/01/030345+08$30.00

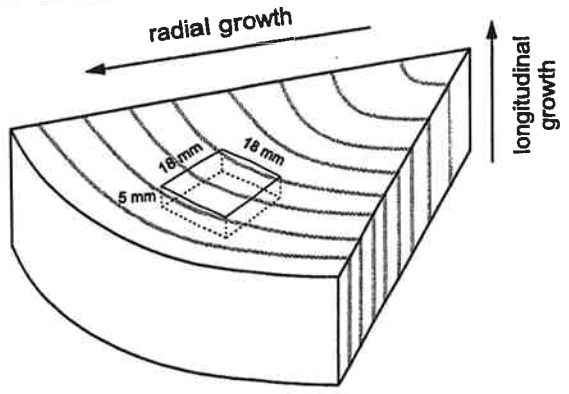

Figure 1. A schematic diagram showing the position of wood samples relative to the tree.

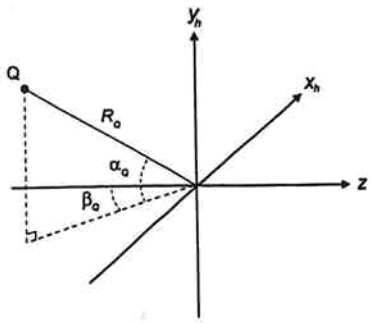

Figure 2. The mean distance variable R_Q and the respective angular variables α_Q and β_Q of the source point Q in hologram imagery. The generalized subscript Q for the variables R, α and β is valid for subscripts for the image (i), reconstruction (c), reference (r) and object (o).

2. Materials and methods

2.1. Sample preparation

The wood material under investigation consisted of 30 randomly selected samples of Scots pine (*Pinus sylvestris L*). In order to minimize the effect of possible differences in moisture content among wood samples, the samples were oven dried for 48 h at 103 °C and stabilized to 12% moisture content. Then samples were sliced transversally to the stem with a double-bladed saw to a final thickness of 5 mm in the longitudinal direction of growth. The other two dimensions of the samples were equal, 18 mm (figure 1). The gravimetric bulk densities, which ranged from 406 to 688 kg m^{-3}, were calculated from the ratio of weight and volume of each sample.

Next, the wood samples were analysed with another corroborating method for our optical study by radiographing them on x-ray negative film [2]. The samples to be radiographed in the longitudinal direction of growth were placed on the film in an envelope. The distance of the film from the source of radiation was 2.5 m and the exposure time was set to 5 min at 23 kV. After the development of the film, the optical densities of the sample images on the x-ray negative film were measured with the aid of a double-beam microdensitometer (Joyce & Loebl). Each sample image was scanned along lines parallel to a radial growth at consecutive spacings of 2 mm. Transmittance responses of the sample images on the film proportional to the extinction of x-ray radiation in respective wood samples were calculated from the formula for the optical density (OD) of the film. The optical density is defined by the formula $OD = \log_{10}(I_i/I_t)$, where I_i and I_t are the intensities of the incident and transmitted light, respectively.

2.2. The theory of the DOE sensor

The imaging properties of the DOE sensor obey the laws of hologram imagery. Thus we can write the mean distance variable of the image R_i as a function of R_c, R_r and R_o and the respective angular variables of the image α_i and β_i as functions of α_c, β_c, α_r, β_r, α_o and β_o as presented in [10, 11] and in figure 2. The generalized subscript Q for the variables is valid for subscripts of the image (i), reconstruction (c), reference (r) and object (o). Let us denote the optical axis and the hologram plane the z axis and x_h–y_h plane, respectively. The variable α describes the angle between the mean position vector R_Q and its projection located on the x_h–z plane, whereas the variable β describes the angle between the z axis and the projection of R_Q on the x_h–z plane. For the present sensor the reference source was at infinity and the respective angular variables α_r and β_r were zero. These substitutions reduce the formulae for the mean distance and angular variables for the image to the following forms:

$$\frac{1}{R_i} = \frac{1}{R_c} + \frac{\mu}{R_o} \tag{1}$$

$$\alpha_i = \sin^{-1}(\sin\alpha_c + \mu \sin\alpha_o) \tag{2}$$

$$\beta_i = \sin^{-1}\left(\frac{\sin\beta_c \cos\alpha_c + \mu \cos\alpha_o \sin\beta_o}{\cos\alpha_i}\right) \tag{3}$$

where $\mu = \lambda_c/\lambda_o$ is the ratio of reconstructing and recording wavelengths. The effect of degradation caused by a possible shift in wavelength was eliminated by using the same wavelength for recording and reconstruction [12]. We determined the relative errors for the variables of the image to be

$$\left|\frac{\Delta R_i}{R_i}\right| \leqslant \left|\frac{1}{R_c^2\left(\frac{1}{R_c} + \frac{\mu}{R_o}\right)}\right| \Delta R_c \tag{4}$$

$$\left|\frac{\Delta\alpha_i}{\alpha_i}\right| \leqslant \left|\frac{\cos\alpha_c}{(1-u^2)^{1/2}\sin^{-1}u}\right| \Delta\alpha_c \tag{5}$$

$$\left|\frac{\Delta\beta_i}{\beta_i}\right| \leqslant \left|\frac{-\sin\beta_c\sin\alpha_c + \frac{vu\cos\alpha_c}{\cos(\sin^{-1}u)(1-u^2)^{1/2}}}{[\cos^2(\sin^{-1}u) - v^2]^{1/2}}\right| \Delta\alpha_c + \left|\frac{\cos\beta_c\cos\alpha_c}{[\cos^2(\sin^{-1}u) - v^2]^{1/2}}\right| \Delta\beta_c \tag{6}$$

where $u = \sin\alpha_c + \mu\sin\alpha_o$ and $v = \sin\beta_c\cos\alpha_c + \mu\cos\alpha_o\sin\beta_o$. The perfect reconstructing wavefront that diffracts from the present DOE forms a 4 × 4 light spot matrix in its focal plane as shown in figure 3. When the imaging properties of the DOE sensor are considered in such a manner as to analyse the distortions of the real reconstructing wavefront, we can estimate the distortions of 4 × 4 spots in the DOE sensor image from equations (4)–(6). The curves shown in figures 4(*a*) and (*b*) help us to understand the behaviour of the distances R_i and ΔR_i of the sensor images as a function of the mean distance R_c, whereas the curves in figure 4(*c*) describe the maximum radius of the spot deviations (SD) in

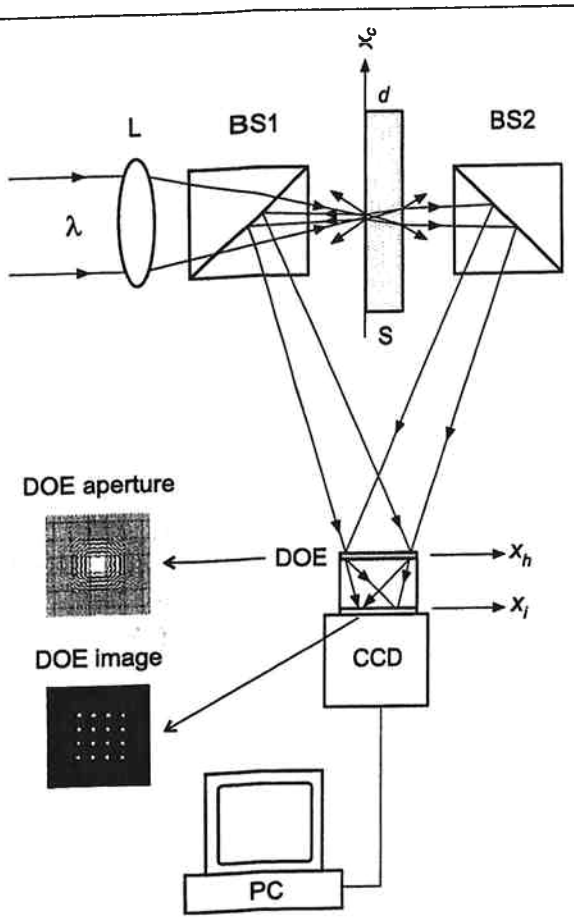

Figure 3. A schematic diagram of the DOE sensor. The expanded wavefront (λ) from the laser is focused by using the lens (L) into the sample (S) with thickness d through a beam splitter (BS1). Beam splitters (BS1 and BS2) guide the reflected and transmitted components of laser light into the DOE aperture (in the x_h–y_h plane), which diffracts the components into its focal plane (the x_i–y_i plane). The amplitude distribution of the DOE aperture and its image with the 4 × 4 light spots are shown in the insets.

the DOE sensor image as a function of R_c for three radii of the scattering pattern of the reconstructing wavefront on the surface of a sample.

2.3. *Realization and use of the DOE sensor*

The DOE, which was calculated by using the Rayleigh–Sommerfeld diffraction integral [13], was an on-axis binary amplitude hologram and its transmission was adjusted to 50%. The coding method used was carrier wave coding. The DOE consisted of a square array of equispaced points as objects. The DOE aperture was 4 mm × 4 mm and the focal length was 100 mm, while the distance between the spots in the focal plane was 125 μm, when R_c was at infinity. The output pattern of the DOE produced a 4 × 4 light spot matrix. The DOE was fabricated using an electron beam writer, which gives the best imaging quality for the DOE. The average signal-to-noise ratio (SNR) in the on-axis reconstruction domain was 21.1 dB. When DOE was used in off-axis reconstruction, as was the case in figure 3 for transmission and reflection mode, the respective SNR was 19.6 dB. The maximum increase of lateral geometrical aberrations caused by the off-axis reconstruction of the DOE was calculated to be less than three wavelengths (1.9 μm), which corresponds to a quarter of the width of the pixel of the CCD.

The reconstructing wavefronts are first scattered from the sample being tested along two optical paths (through BS1 and BS2) and after that they are diffracted from the DOE to its focal plane. Optical diffraction is dominant for the DOE aperture. The effect of optical interference is negligible because the mean distance between the interference fringes caused by wavefronts through BS1 and BS2 is smaller than the minimum feature size of the DOE aperture. Thus, the wavefronts are diffracted into separate locations of the focal plane without overlapping. Sample irregularities distort the wavefronts when they are incident on the sample, leading to the deformation of the images of the spot matrixes. A CCD camera simultaneously captures the deformed image patterns and the images are analysed by a personal computer. To avoid possible interference of the wavefronts travelling through BS1 and BS2 into the DOE aperture, the respective wavefronts can be directed separately through the DOE aperture to perform imaging onto the detector element.

The image of the 4 × 4 light spots when the real wavefront from a single spot in the x_c plane generated by the lens L passes through BS2 is shown in figure 5(*a*), whereas the intensity distribution of the same spot image plotted in the x_i direction is shown in figure 5(*b*). When a semitransparent mirror of optical quality with an optical density of 4 was inserted into the sample cell, the image of the light spots (figures 5(*c*) and (*d*)) exhibited distributions rather similar to those in the case of the real wavefront in figures 5(*a*) and (*b*).

Next, we will consider the imaging of the DOE sensor with wood samples. Scattering from a wood sample (reflection mode) and through a wood sample (transmission mode) will change the direction of the photons from that in the perfect wavefront. Here we present two examples in which the reconstructing wavefront is scattered through a wood sample in longitudinal (figure 6(*a*)) and in radial (figure 6(*b*)) directions of growth of a stem. In the longitudinal direction, the scattering pattern of the reconstructing wavefront exhibits a rather circular shape for x_c and y_c directions at the location $z_c + d$. This is caused by the scattering through the cell walls and cell cavities parallel to the longitudinal axes of the grains of wood, whereas, in the radial direction, cell walls and cell cavities act as bundles of scattering optical waveguides stretching the scattering pattern of the reconstructing wavefront observed on the surface of a sample. Thus it is obvious that the shape of the scattering pattern on the sample surface is related to the orientation of the wood grains. When the scattering patterns on the surface of the samples shown in figures 6(*a*) and (*b*) are imaged by the DOE sensor, one can observe the respective images shown in figures 6(*c*) and (*d*). Similar shapes of scattering patterns on the surface of the samples with strong specular components can be observed in reflection mode. When the scattering patterns with strong specular components on the surface of the samples are imaged with the DOE sensor, one can observe a bright 4 × 4 spot matrix in the DOE image. If the bright specular spots were rejected from the DOE image, weighting in the direction of scattering could be analysed from the images.

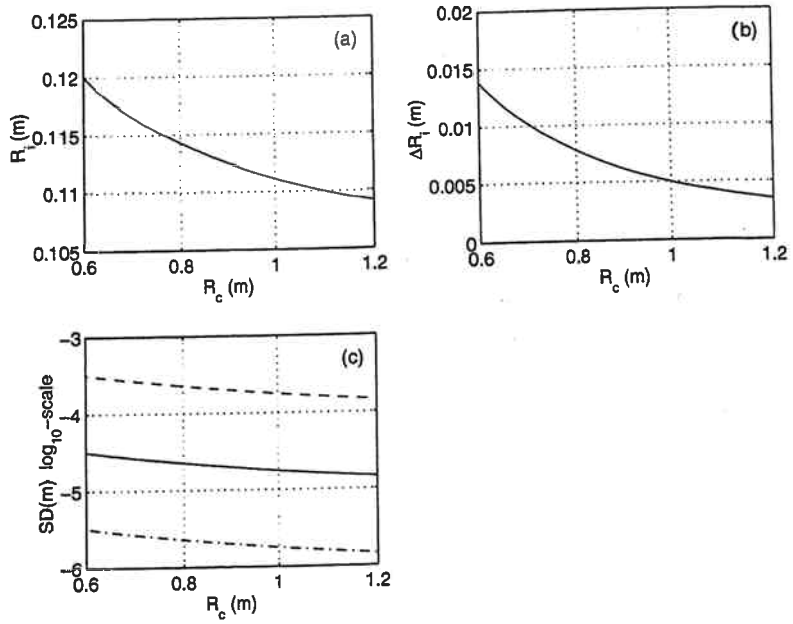

Figure 4. (*a*) The mean distance variable of the image R_i, (*b*) its error ΔR_i for sample thickness $d = 5$ mm and (*c*) the maximum radius of the spot deviation (SD) in the image as a function of the mean distance R_c. In (*c*) the three curves of maximum radius of the SD are calculated to represent the radii ($\rho_1 = 0.16$ mm (chain line), $\rho_2 = 1.60$ mm (full line) and $\rho_3 = 16$ mm (broken line)) of the scattering pattern of the reconstructing wavefront on the surface of a sample.

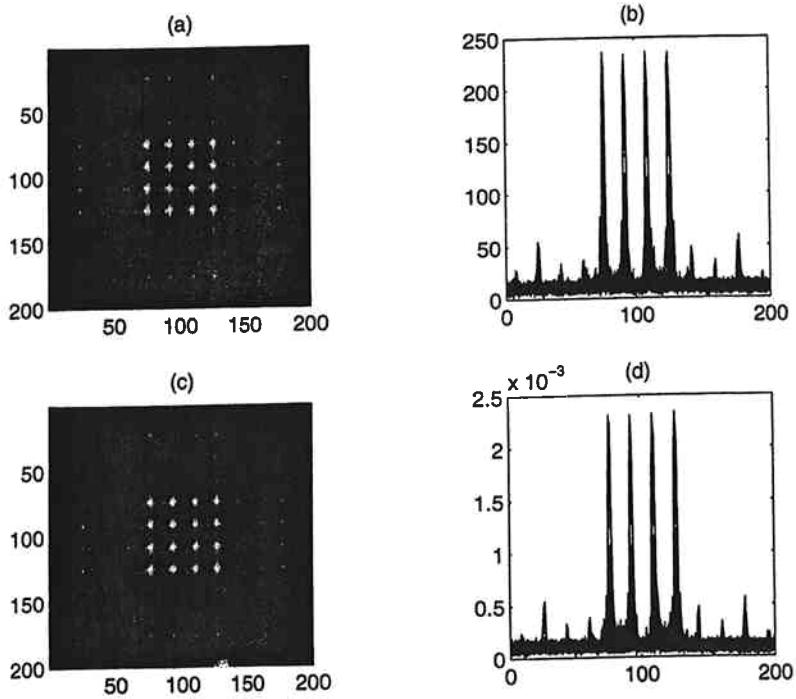

Figure 5. The DOE image patterns obtained by using the DOE sensor set-up of figure 3 (through BS2). The 4 × 4 spot image for a real wavefront (*a*) and with a semitransparent mirror (OD = 4) as a sample (*c*) and their respective intensity plots in the x_i direction (*b*) and (*d*). The numbers shown on the axes are pixel numbers: in (*a*) and (*c*) they are for distance, whereas vertical axes of (*b*) and (*d*) are for intensity and horizontal axes for distance.

3. Results

We measured the total reflectance and transmittance in the longitudinal direction of growth of the wood samples in the wavelength range 200–850 nm by using a Perkin Elmer λ18 spectrophotometer (with an integrating sphere). In order to reduce the effect of scattering of light from the sample edges, we used a mask with a circular aperture (of diameter 15 mm) during the measurements. The calculated spectral limits in reflectance and in transmittance for all 30 samples using minimum and maximum values of the sample responses at 1 nm intervals are shown in figure 7. Next we

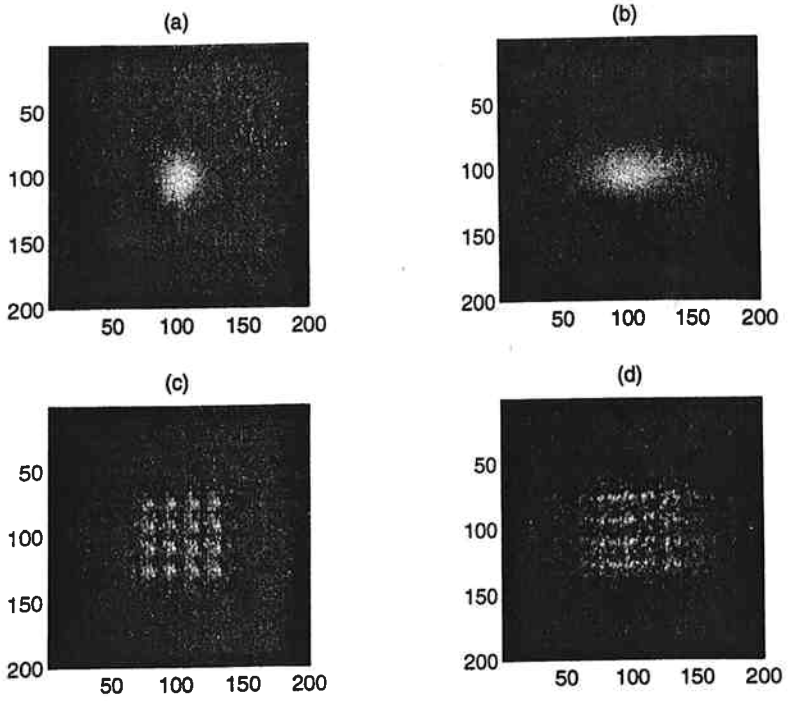

Figure 6. Patterns of the reconstructing wavefront scattered through a 1.2 mm thick wood sample at its back surface in (*a*) longitudinal and (*b*) radial directions of growth, and the respective DOE sensor images (*c*) and (*d*). The numbers shown on the axes are pixel numbers.

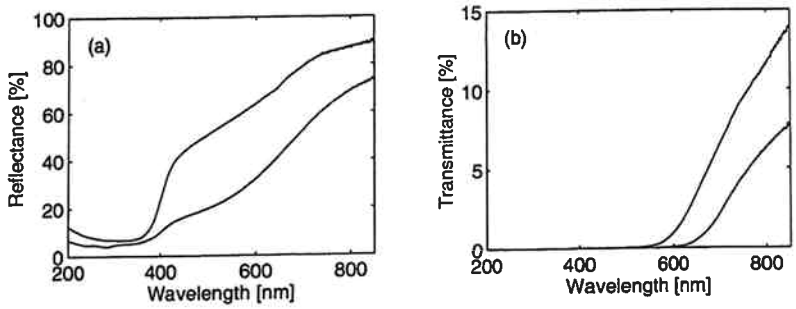

Figure 7. Maximum and minimum limits of the spectrophotometer responses for the 30 wood samples at 1 nm intervals: (*a*) reflectance and (*b*) transmittance. (Note that maximum and minimum limits in reflectance and transmittance do not necessarily represent any individual sample and thus the local sum of reflectance and transmittance can exceed 100%.)

calculated consecutively correlation coefficients relating the bulk density and spectral reflectance and transmittance by using Pearson product-moment correlation, which was used for calculations of all correlations mentioned later in this paper. The correlations for reflectance exhibit an increasingly negative correlation as a function of wavelength, which can be observed in figure 8(*a*), whereas the respective correlations for the transmittance indicate that there is an increasingly high correlation at longer wavelengths (figure 8(*b*)). The fluctuation of correlations for transmittance in the wavelength region 200–500 nm is caused by high absorption and negligible transmittance, as one can observe in figure 7(*b*).

From the highest correlation for both reflectance and transmittance in the wavelength range 800–850 nm, as shown in figures 8(*a*) and (*b*) and in table 1, we calculated the mean values for reflectance and transmittance in that wavelength range for each of 30 wood samples. The values as a function of the bulk density are plotted in figures 9(*a*) and (*b*), with the root mean square line fits. Next, the measured optical density values from the x-ray negative film for the same area of sample as that used in spectrophotometric measurements were converted to the respective transmittance values (figure 9(*c*)). The correlation between the bulk density and the transmittance of sample images on the x-ray negative film was calculated to be 0.923, as shown in table 1. Next, we applied a semiconductor laser ($\lambda = 980$ nm) to measure the reflectance and transmittance of our wood samples at longer wavelengths as was the case in spectrophotometer measurements. The results obtained were correlated to the bulk density of the wood samples (table 1).

In the next step, we investigated the reflectance and transmittance properties of the wood sample by using the DOE sensor. The laser beam of a 17 mW He–Ne laser ($\lambda = 632.8$ nm) was focused by a lens ($f = 200$ mm) onto the surface of a wood sample parallel to its longitudinal direction of growth (figure 3). The diameter of the waist of the focused beam on the surface of the wood sample was calculated

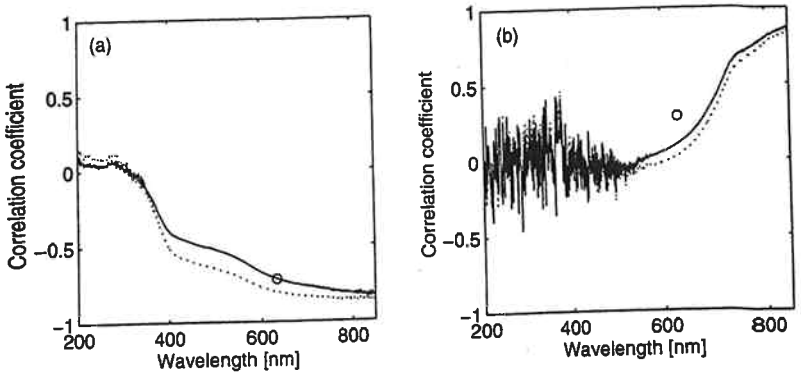

Figure 8. Correlations (full line) between the bulk density of the 30 samples and the spectral reflectance (*a*) and transmittance (*b*). The respective spectral correlation to the transmittance of sample images on the x-ray negative film is indicated by a dotted line. The correlation between the bulk density and the mean image intensities of the DOE sensor is indicated by open circles.

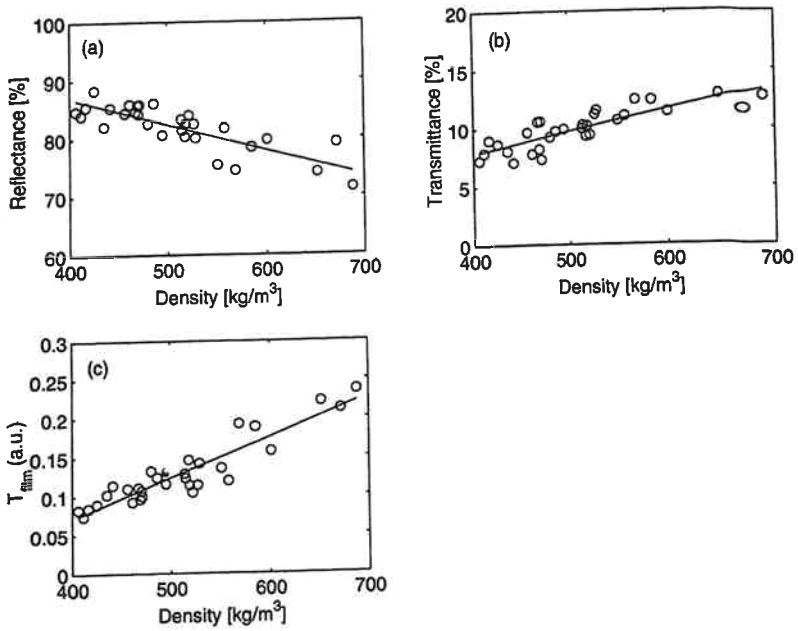

Figure 9. The mean reflectance (*a*) and transmittance (*b*) as functions of the bulk density of the 30 wood samples for the wavelength range 800–850 nm. The mean transmittance of sample images on x-ray negative film is shown as a function of the bulk density (*c*).

Table 1. Correlation coefficients relating bulk density data of samples and the data obtained by using a spectrophotometer, a semiconductor laser and radiography.

	Spectrophotometer, λ = 800–850 nm	Semiconductor laser, λ = 980 nm	Radiography
Reflectance	−0.827	−0.870	
Transmittance	0.839	0.715	0.923

to be 160 μm, whereas the diameter of the beam scattered through the sample was measured to be approximately 2 mm at the $1/e^2$ level. The DOE sensor was located 900 mm from the sample. The reflected and transmitted signals were diffracted through the DOE aperture and the DOE images were simultaneously detected with the chip of the CCD camera. The CCD camera was located 112.5 mm from the DOE aperture, as one can calculate from equation (1) and observe in figure 4(*a*). The system records the specularly and diffusely scattered components that are simultaneously incident on the sensor aperture. The specular component is related to the image of the 4 × 4 spots, whereas diffuse scattering can be observed in the formation of speckle patterns.

Different images were obtained by performing stepwise scans for each wood sample. This was accomplished by measuring the specular and diffuse components of the scattered light of the samples at 100 μm intervals along the three lines with 2 mm parallel spacing over the specimen. From the set of the images a mean image pattern was calculated. The correlation between the bulk density and change in intensity of the mean image of the DOE sensor for each sample is indicated by an open circle in figures 8(*a*) and (*b*). The correlation

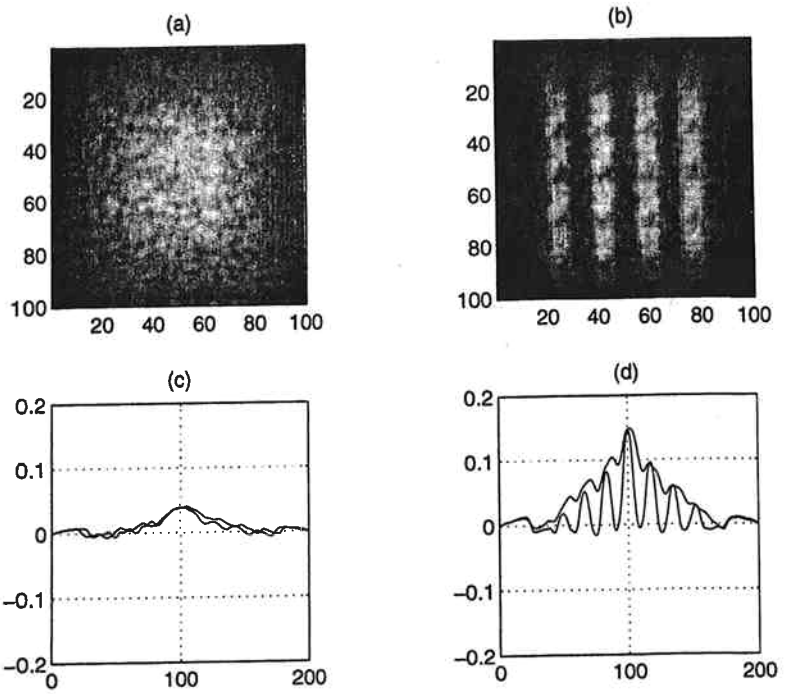

Figure 10. The intensity patterns of the DOE sensor image scattered through a 5 mm thick layer of (*a*) earlywood and (*b*) latewood. The respective x and y projections from the two-dimensional cross-correlation patterns between the image of a transparent sample without insertion losses and the image of (*a*) and the image of (*b*) are shown in (*c*) and (*d*) respectively.

between spectrophotometric data and the transmittance data of the sample images on the x-ray negative film is also shown for reflectance (figures 8(*a*)) and for transmittance (figure 8(*b*)) as dotted lines.

We also investigated the anisotropy of the wood samples by analysing the intensity patterns of the DOE sensor images produced by using laser light components, which were scattered through earlywood and latewood regions. The differences between DOE sensor images from earlywood and latewood are shown in figure 10. In the case of earlywood, we were not able to observe the 4×4 spot image for $R_c = 900$ mm (figure 10(*a*)). This probably resulted from the fact that the cell walls are thin and the cell cavities are large in the earlywood region. Thus, the scattering of light from the earlywood region is rather diffuse. In the latewood region one can observe a higher visibility of the spots in the x than in the y direction, as shown in figure 10(*b*). In the latewood region the cell walls are thicker and cell cavities smaller than they are in the earlywood region. This is also the main reason for the variation in density between early and latewood. To investigate the optical anisotropy of the wood structure inside a year ring we used a two-dimensional cross-correlation analysis. For the reference of the two-dimensional analysis we cross-correlated the images to those for a transparent sample without insertion losses. The difference in results due to a variation in wood structure between earlywood and latewood can be observed from the x and y projections of the correlated images, as shown in figures 10(*c*) and (*d*).

4. Conclusions

We have investigated the spectral reflectance and transmittance of dried Scots pine (*Pinus Sylvestris L*) wood samples and compared the measured spectra with the bulk density. The Pearson product-moment correlation between the bulk density and optical signals exhibited the highest correlation at wavelengths from 800 to 850 nm, when the wavelength range from 200 to 850 nm was used. A similar observation was made at the wavelength of 980 nm of a semiconductor laser. This may indicate that the correlation between the bulk density and the optical signal is also high at wavelengths longer than 850 nm. In order to find the most suitable range of wavelength, further research is needed. On the other hand, the correlation between the bulk density and radiographic data was not significantly higher than that between the bulk density and the spectrophotometric data. This difference in correlation may result from the stronger influence of optical activity, birefringence and polarization on optical than on x-ray signals, so further research is needed in order to determine the specific influences of each factor.

The correlations between the bulk density and the intensity of the DOE sensor images at a wavelength of 632.8 nm were in accordance with the correlations obtained by spectrophotometry. However, spectrophotometry as a method is incapable of sensing the local anisotropy of wood material. We state that the DOE sensor can distinguish anisotropy of the wood structure in the radial as well as in the longitudinal direction of growth, including the variations of anisotropy in intra-ring regions. Investigations of the intra-ring variation in wood structure with the DOE sensor will be a part of our further research.

Acknowledgments

JP thanks the Jenny and Antti Wihuri Foundation and JP and RS thank the Academy of Finland for financial support.

The authors express their special thanks to Seppo Kellomäki and Heli Peltola from the Faculty of Forestry, University of Joensuu, Finland and to Kari Sauvala from the Finnish Forest Research Institute for useful discussions.

References

[1] Tsoumis G 1991 *Science and Technology of Wood: Structure, Properties, Utilization* (New York: Chapman & Hall) pp 111–25
[2] Saikku O 1975 *Commun. Inst. For. Fenn.* **85** 1–49
[3] Kellomäki S 1979 *Silva Fenn.* **13** 304–15
[4] Hakkila P 1979 *Commun. Inst. For. Fenn.* **96** 1–59
[5] Attaelman A, Larsson S, Rindby A and Voglis P 1994 *Rev. Sci. Instrum.* **65** 7–12
[6] Barbour R J, Johnson J and Amundson C 1996 Modeling intraring x-ray density profiles *Second Workshop on Connection Between Silviculture and Wood Quality through Modeling Approaches and Simulation Softwares, Berg-en-Dal, Kruger National Park, South Africa, August 26–31* pp 123–30
[7] Silvennoinen R, Peiponen K-E and Asakura T 1999 Diffractive optical elements in material inspection *The International Trends in Optics and Photonics ICO IV, Part VI Optical Metrology* ed T Asakura (Berlin: Springer) pp 282–93
[8] Silvennoinen R, Peiponen K-E, Räsänen J, Sorjonen M, Keränen E, Eiju T, Tenjimbayashi K and Matsuda K 1998 *Opt. Eng.* **37** 1482–7
[9] Silvennoinen R, Palviainen J, Kellomäki S, Peltola H and Sauvala K 1999 Detection of wood density by a diffractive optics based sensor *Proc. XVIII Congress of the Int. Commission for Optics, San Francisco, California, USA, August 2–6* pp 312–3
[10] Latta J N 1971 *Appl. Opt.* **10** 599–608
[11] Latta J N 1971 *Appl. Opt.* **10** 609–18
[12] Roux F S 1994 *Opt. Eng.* **33** 2843–8
[13] Nieto-Vesperinas M 1991 *Scattering and Diffraction in Physical Optics* (New York: Wiley)